Bioactive Materials 6 (2021) 3449–3460

Contents lists available at ScienceDirect

Bioactive Materials

journal homepage: www.sciencedirect.com/journal/bioactive-materials

Fibroblasts upregulate expression of adhesion molecules and promote lymphocyte retention in 3D fibroin/gelatin scaffolds

Maxim A. Nosenko [a,*], Anastasia M. Moysenovich [b], Anastasia Y. Arkhipova [b,c], Kamar-Sulu N. Atretkhany [a], Sergei A. Nedospasov [a,b,d], Marina S. Drutskaya [a], Mikhail M. Moisenovich [b]

[a] Center for Precision Genome Editing and Genetic Technologies for Biomedicine, Engelhardt Institute of Molecular Biology, Russian Academy of Sciences, Moscow, 119991, Russia
[b] Biological Faculty, Lomonosov Moscow State University, Moscow, 119991, Russia
[c] Biological Faculty, Shenzhen MSU-BIT University, Shenzhen, 518172, China
[d] Sirius University of Science and Technology, Federal Territory Sirius, Krasnodarsky Krai, 354340, Russia

ARTICLE INFO

Keywords:
Bioengineering
Cell adhesion
Artificial lymphoid tissue
Mouse embryonic fibroblasts
Stromal cells
TNF
ICAM-1
VCAM-1
JNK
Fibroin/gelatin
3D
2D

ABSTRACT

Bioengineered scaffolds are crucial components in artificial tissue construction. In general, these scaffolds provide inert three-dimensional (3D) surfaces supporting cell growth. However, some scaffolds can affect the phenotype of cultured cells, especially, adherent stromal cells, such as fibroblasts. Here we report on unique properties of 3D fibroin/gelatin materials, which may rapidly induce expression of adhesion molecules, such as ICAM-1 and VCAM-1, in cultured primary murine embryonic fibroblasts (MEFs). In contrast, two-dimensional (2D) fibroin/gelatin films did not show significant effects on gene expression profiles in fibroblasts as compared to 3D culture conditions. Interestingly, TNF expression was induced in MEFs cultured in 3D fibroin/gelatin scaffolds, while genetic or pharmacological TNF ablation resulted in diminished ICAM-1 and VCAM-1 expression by these cells. Using selective MAPK inhibitors, we uncovered critical contribution of JNK to 3D-induced upregulation of these adhesion molecules. Moreover, we observed ICAM-1/VCAM-1-dependent adhesion of lymphocytes to fibroblasts cultured in 3D fibroin/gelatin scaffolds, but not on 2D fibroin/gelatin films, suggesting functional reprogramming in stromal cells, when exposed to 3D environment. Finally, we observed significant infiltration of lymphocytes into 3D fibroin/gelatin, but not into collagen scaffolds *in vivo* upon subcapsular kidney implantation in mice. Together our data highlight the important features of fibroin/gelatin scaffolds, when they are produced as 3D sponges rather than 2D films, which should be considered when using these materials for tissue engineering.

1. Introduction

Artificial tissue and organ engineering represents rapidly evolving research field, which may provide new therapeutic opportunities in the treatment of various diseases ranging from complete replacement of missing or damaged organ to tissue-specific delivery of cells, growth factors, vaccines, or drugs *in vivo* using bioengineered carriers [1–3]. One potential application of this approach is generation of artificial lymphoid tissues capable of attracting host-derived immune cells and inducing antigen-specific immune response. Such artificial organoids represent attractive tools for cancer immunotherapy [4,5] as well as for routine vaccinations [6]. However, there remain several unresolved issues regarding artificial lymphoid tissue generation with the key focus on the reconstruction of stromal and immune cell interactions.

Organ functionality requires cells to undergo a specific spatial distribution in the three-dimensional (3D) extracellular matrix (ECM) [7]. In order to reproduce this distribution in artificial tissues, various bioengineered 3D scaffolds have been developed [8–10]. Several types of biomaterials are considered suitable for scaffold production including synthetic [11,12] and natural [13] biopolymers. Physical and chemical properties of such biomaterials determine the bioactivity of fabricated scaffolds and can affect the expression program of the cells that interact

Peer review under responsibility of KeAi Communications Co., Ltd.
* Corresponding author.
E-mail address: maxim-nosenko@yandex.ru (M.A. Nosenko).

https://doi.org/10.1016/j.bioactmat.2021.03.016
Received 14 September 2020; Received in revised form 5 February 2021; Accepted 4 March 2021

with the scaffold [14–17]. For example, hydroxyapatite is attracting much attention because for its osteogenic properties [18], while tantalum-based 3D scaffolds support hematopoietic differentiation of embryonic stem cells [19]. Both synthetic and natural types of scaffolds are potentially being applicable for tissue engineering with specific tasks.

Despite the growing number of studies involving silk-based biomaterials, there is still a gap in our understanding of how these materials affect cell properties. Recent study demonstrated proinflammatory phenotype of human monocytes cultured on 3D fibroin scaffolds [20]. In line with that, proinflammatory properties of fibroin/gelatin, but not spidroin microparticles in the model of skin wound healing in mice were also reported [21]. In addition, an increase in ICAM-1 expression by murine embryonic fibroblasts (MEFs) cultured in 3D fibroin/gelatin scaffolds for several weeks were previously observed, although the exact mechanism for this effect was not defined [22]. In this study we uncover a peculiar property of 3D, but not of 2D fibroin, supplemented with gelatin, to induce a rapid expression of the adhesion molecules ICAM-1 and VCAM-1 in the primary cultured MEFs. These changes in stromal cell expression programs promote lymphocyte adhesion and retention in 3D fibroin/gelatin scaffolds both *in vitro* and *in vivo*. Together our data indicate that 3D fibroin/gelatin scaffolds can be beneficial for engineering of artificial lymphoid organs or for generation of biomaterial-based vaccines.

2. Materials and methods

2.1. Scaffold fabrication

Scaffolds were prepared from aqueous fibroin and gelatin solutions with minor modifications from previously described protocol [23]. Briefly, silk surgical threads (LCC "Optikum") were boiled for 1.5 h in 0.03 M $NaHCO_3$ (pH 8.4), washed in distilled water and dried in order to remove resediual sericin. Sericin-free silk was dissolved in a mixture of $CaCl_2$:C_2H_5OH:H_2O (1:2:8 M proportion) for 5 h in water bath at 50 °C. Dissolved fibroin was centrifuged at 13,000 g and dialyzed using D14 dialysis membrane (MWCO -12000 M, Orange scientific) against distilled water at 20 °C. After 10 dialysis cycles the solution was centrifuged for 20 min at 13,000 g.

Two-dimensional (2D) scaffolds were prepared using solution-casting method. Fibroin/gelatin (7:3) as 2% aqueous solution was applied as a thin layer to the surface of 35 mm culture dish and dried at room temperature for 2 days. Dried 2D fibroin/gelatin films were placed in 96% ethanol for 1 h, followed by gradual transfer to distilled water with decreased alcohol concentration by 10% every 15 min.

Three-dimensional scaffolds, 15 mm in diameter and 3.5 mm thick, were prepared in 24-well plates by adding 700 μL of 2% aqueous fibroin/gelatin (7:3) solution (3D F/G scaffolds) or 2% gelatin solution (3D G scaffolds) supplemented with 1% DMSO to each well. The plates were then stored at −20 °C for 7 days. Frozen scaffolds were soaked in 96% ethanol for 1 h, then samples were removed from the wells and transferred to 70% ethanol for storage. For implantation experiments 3D scaffolds were fabricated according to the same protocol, but employing 4 mm diameter plastic tube for casting. To generate F/G disks for implantation the resulting tube-shaped scaffolds were then cut to the final thickness of 1.5 mm and the diameter of 4 mm. 3D polystyrene scaffolds were purshased from Merck Sigma Aldrich. 3D collagen scaffolds were purshased from Advanced Biomatrix.

2.2. Mice

WT, TNF-deficient (TNF KO) [24] and IL-6-deficient (IL-6 KO) mice (generated from those described in Ref. [25]) on C57BL/6 genetic background were provided by the SSU "Biomodel," a branch of the Shemyakin and Ovchinnikov Institute of Bioorganic Chemistry, Russian Academy of Sciences, housed under specific pathogen-free conditions on 12 h light/dark cycle at 20–23 °C and used for the experiments at the age of 8–10 weeks (weight of 20–22 g). GFP-transgenic mice (C57BL/6-Tg (CAG-EGFP)1Osb/J, The Jackson Laboratory) were kindly provided by Dr. N. Logunova from the Central Scientific Research Institute of Tuberculosis, Moscow, Russia. Animal manipulations were carried out in accordance with recommendations in the Guide for the Care and Use of Laboratory Animals (NRC 2011), the European Convention for the Protection of Vertebrate Animals Used for Experimental and Other Scientific Purposes, Council of Europe (ETS 123), and "The Guidelines for Manipulations with Experimental Animals" (the decree of the Presidium of the Russian Academy of Sciences of April 2, 1980, no. 12000–496).

2.3. Mouse embryonic fibroblasts cultures

Primary mouse embryonic fibroblasts (MEFs) were isolated from WT, TNF KO, IL-6 KO and GFP-transgenic mice according to standard protocol [26]. Cells were cultured on 10 cm culture dishes for adherent cells (Greiner bio-one) in 10 mL of DMEM (ThermoFisher), supplemented with 100 U/mL of penicillin, 100 μg/mL of streptomycin, 2 mM L-glutamine, and 10% fetal bovine serum (all from ThermoFisher). To detach the cells from the dish, 0.25% trypsin 2 mM EDTA solution (ThermoFisher) was used. For experiments MEFs were seeded on 24-well plates in different conditions: standard culture plate (control), 2D F/G films (2D), or 3D scaffolds, fabricated from fibroin (3D F), gelatin (3D G), fibroin/gelatin (3D F/G) or polystyrene (3D PS, Merck). First, 2×10^5 cells were transferred to each scaffold in 100 μL of medium and placed in incubator for 1 h to promote cell attachment. Then 900 μL of the medium were added to each well, resulting in 1 mL sample volume. For control and 2D F/G culture conditions 2×10^5 cells/well in 1 mL total volume were seeded on standard of F/G-treated 24-well plates, respectively. At certain timepoints, culture medium was collected to analyze cytokine production, and scaffolds with cells were harvested in TriZol (ThermoFisher) for mRNA expression analysis. In supernatant transfer experiments culture medium from control, 2D- or 3D-cultured MEFs was collected at specified timepoints and placed over cells cultured under control conditions. In this case, cells were harvested using TriZol for mRNA analysis following 6 h of culture with transferred supernatants.

2.4. Lymphocyte adhesion assay

Mice, 6 to 8 weeks old, were euthanized by cervical dislocation and their spleens were collected into sterile RPMI1640 (ThermoFisher). Single cell suspensions were obtained by mashing the spleen and passing cells through 30 μm pre-separation filter (Miltenyi Biotec Inc.). For positive magnetic separation of $CD4^+$ cells, splenocytes were incubated with L3T4 Microbeads (Miltenyi Biotec Inc.) for 15 min at 4 °C. After this, cells were treated with Cy3-conjugated secondary polyclonal antibodies (goat anti-rat IgG H + L) for 5 min at 4 °C. Cells were then washed once with PBS containing 0.5% BSA and 2 mM EDTA (pH 7.2). The amount of antibodies and beads were determined based on the initial cell count according to manufacturer's protocol. Cells were maintained in chilled PBS containing 0.5% BSA and 2 mM EDTA (pH 7.2) throughout the incubations. For all magnetic cell separations, cells were transferred to LS Columns (Miltenyi Biotec Inc.) and MidiMACS following manufacturer's instructions. Labeled cells were collected as the positive fraction for subsequent experiments.

Primary GFP^+ MEFs were seeded at 2×10^5 cells/well on 2D F/G-coated glass slides or in 3D F/G scaffolds and cultured for two days. The culture medium was then replaced and 2.5×10^5 of $CD4^+$ cells were added to each well 16 h later. After 4 h of co-culturing MEFs with $CD4^+$ cells at 37 °C and 5% CO_2, non-adherent cells were removed and the scaffolds were washed five times with DMEM to further eliminate unbound or loosely-bound cells. Samples were fixed with 4% paraformaldehyde and stained with DAPI (Thermo Fisher Scientific). Images were captured using Eclipse Ti-E microscope with the A1 confocal

Table 1
Primer sequences for RT-PCR.

Gene	Forward primer 5′-3′	Reverse primer 5′-3′
Actb	CTCCTGAGCGCAAGTACTCTGTG	TAAAACGCAGCTCAGTAACAGTCC
Icam1	AGTGGGTCGAAGGTGGTTCT	TCCAGCCGAGGACCATACAG
Vcam1	GACAGCCCACTAAACGCGAA	TCCTTGGGGAAAGAGTAGATGTCC
Tnf	TAGCCCACGTCGTAGCAAAC	ACAAGGTACAACCCATCGGC
Il6	AACCACGGCCTTCCCTACTT	TTGCCATTGCACAACTCTTTTCTC
Icam2	ATTTCAGTTGGGAGCGCCAG	CCAGACCCTGGGCTGTAGAA
Icam4	CTGCTTACAAACGGCCCAGAA	CACTCGGCCACCTCTTCTCA
Icam5	CTGATTCGCCGCAGTTTCGT	GGAGGCATGGCAAAGGTACG
Itgb1	GGACGCTGCGAAAAGATGAATTTG	CCGCAAGATTTGGCATTTGCT
Itgb2	GTGTCCCAGGAATGCACCAA	GTCCAGTGAAGTTCAGCTTCTGG
Itga4	AAGCGAGGTGCAGACCGA	CCCCACGATGAGCCAGC
Itgal	ACTTCCACTTCCCGATCTGCAT	CTGTGTGGATTGAAGGTCTCAGG
Vegfa	CCGAGCCGGAGAGGGAG	GCAGCCTGGGACCACTTG
Vegfb	TGAAGCCAGACAGGGTTGC	GGATGATGTCAGCTGGGGAG
Vegfc	GGTCCATCCACCATGCACTT	TTGCCTTCAAAAGCCTTGACC
Kdr	GCATACCGCCTCTGTGACTT	TCGCCAGGCAAACCCAC
Flt1	CATCCCTCGGCCAACAATCA	CACCAATGTGCTAACCGTCTTATT
Flt4	ATTATCCAGGGAAGCAGGCAG	CGCTGAATCCCATTGTTGGC
Cxcl13	CTCTCTCCAGGCCACGGTATT	CCAGGGGGCGTAACTTGAAT

module (Nikon Corporation) and Plan Fluor 40×1.3 objective. Image analysis was performed using NIS-Elements and ImageJ software [27]. To determinate the role of adhesion molecules in MEF–$CD4^+$ cell interactions, MEFs were pre-exposed to 20 μg/mL monoclonal antibodies against ICAM-1 (KAT1) or VCAM-1 (6C71) (generously provided by Dr. A. Kruglov, DRFZ, Berlin, Germany) for 45 min at 37 °C and 5% CO_2 prior to co-culturing them with $CD4^+$ cells. 2D-cultured MEFs and non-seeded scaffolds were used as controls. All experiments were performed in duplicate wells.

2.5. Kidney subcapsular implantation

F/G or collagen (Advanced Biomatrix) scaffolds (4 mm in diameter) were used for implantation studies. Some scaffolds were first colonized with MEFs (10^4 cells/scaffold) and cultured in complete DMEM in 96-well plates (200 μL of medium per sample) for one day. Control blank scaffolds without the cells were also cultured in the same medium for one day prior to implantation. On the day of implantation scaffolds were washed 3 times in 1 mL of sterile PBS prior to the start of surgical procedures. Implantation was performed according to the published protocol [28]. WT mice were anesthetized with 100 μL of 10% Zoletil/20% Rometar mixture in PBS and kept on heating pad until complete recovery from anesthesia. Each scaffold was cut in two equal parts, which were subsequently implanted under the kidney capsule (maximum 2 implants per kidney and total of 4 implants per mouse) and surgical sutures (Sterion, Russia) were applied to close the wounds. Three weeks following the implantation mice were euthanized and implanted scaffolds were collected and frozen in OCT Tissue Tech compound for subsequent IHC analysis. Some of the scaffolds were snap frozen in liquid nitrogen for subsequent gene expression analysis.

2.6. Intracellular signaling pathway inhibitors

MAPK inhibitors were purchased from Cell Signaling Technology: 10 μM of U0126 was used to inhibit ERK1/2, 50 μM of SP600125 was used to inhibit JNK 1/2 and 10 μM of SB202190 was used to inhibit p38. In addition, 20 μM of JSH-23 (SigmaAldrich) was used to inhibit classical NFκB activation. All inhibitors were prepared as 1000x stock solutions in DMSO, thus, 0.1% DMSO was added to the control group. MEFs were exposed to the corresponding inhibitors for 30 min prior to being transferred to the scaffolds. Following 6-h incubation cells were harvested for gene expression analysis.

2.7. TNF inhibition

Murine TNF neutralizing antibody (clone XT3.11, BioXCell) and rat IgG1 isotype control (clone TNP6A7, BioXCell) were used at concentration of 2 μg/mL in the experiments with TNF inhibition. Antibodies were added at the time when cells were seeded on 3D F/G scaffolds or culture plate. After 6 h of incubation cells were harvested for gene expression analysis.

2.8. Gene expression analysis

RNA was isolated using TriZol (ThermoFisher) according to manufacturer's instructions. RNA quantity and purity were analyzed by measuring A260, A230, and A280 using NanoPhotometer N50 (IMPLEN). For each sample, 1 μg of RNA was treated with DNase I (ThermoFisher) and subsequently used for reverse transcription with oligo-(dT) primers (ThermoFisher). Gene expression analysis was performed using RT-PCR kit (Evrogen) on 7500 RT-PCR System Machine (Applied Biosystems). Primer sequences specific for exon-exon junctions of the target genes were designed using NCBI PrimerBlast software and are listed in Table 1. *Actb* gene was used as internal reference. RT-PCR quality check was performed using melting curve analysis. Data analysis was performed using $2^{-\Delta\Delta Ct}$ method [29]. In most cases, expression levels relative to control standard culture conditions are shown, unless otherwise stated.

Table 2
Antibodies for immunofluorescent staining.

Target	Fluorophore	Clone	Dilution	Supplier
ICAM-1	Cy5	KAT1	1:300	DRFZ*
VCAM-1	FITC	6C71	1:200	DRFZ*
CD4	–	RM4-5	1:200	BD
CD3	–	145-2C11	1:400	ThermoFisher
B220	–	RA3-6B2	1:400	BD
CD31	–	390	1:400	BD
F4/80	–	BM8	1:400	ThermoFisher
rat IgG	Alexa Fluor 546	polyclonal	1:200	Jackson ImmunoResearch
hamster IgG	Alexa Fluor 488	polyclonal	1:200	Jackson ImmunoResearch
rabbit IgG	Alexa Fluor 647	polyclonal	1:200	Jackson ImmunoResearch

* - Kindly provided by Dr. A. Kruglov, DRFZ, Berlin, Germany.

2.9. Immunofluorescent staining

Samples of 3D F/G scaffolds or 2D F/G films with MEFs were fixed in 4% PFA and washed in PBST (PBS buffer with 0.1% Triton-X100) for 10 min. Next, non-specific binding was blocked with 0.3 M glycine, 1% BSA in PBST for 2 h. Primary antibodies to ICAM-1 and VCAM-1 (see Table 2) and SYTOX orange dye (3.125 μM, ThermoFisher) were added in PBST supplemented with 0.3 M glycine and 1% BSA and incubated for 45 min. After three washes in PBST, samples were mounted in Aqua-Poly/Mount (Polysciences, Inc.) and analyzed using confocal microscope Nikon Eclipse Ti-E A1 (Nikon Corporation) and objective lens CFI Plan Apo VC 20x/0,75.

Implanted scaffolds were fixed in 4% PFA and placed on a shaker for 30 min at +4 °C. Samples were then washed in PBST and blocked in

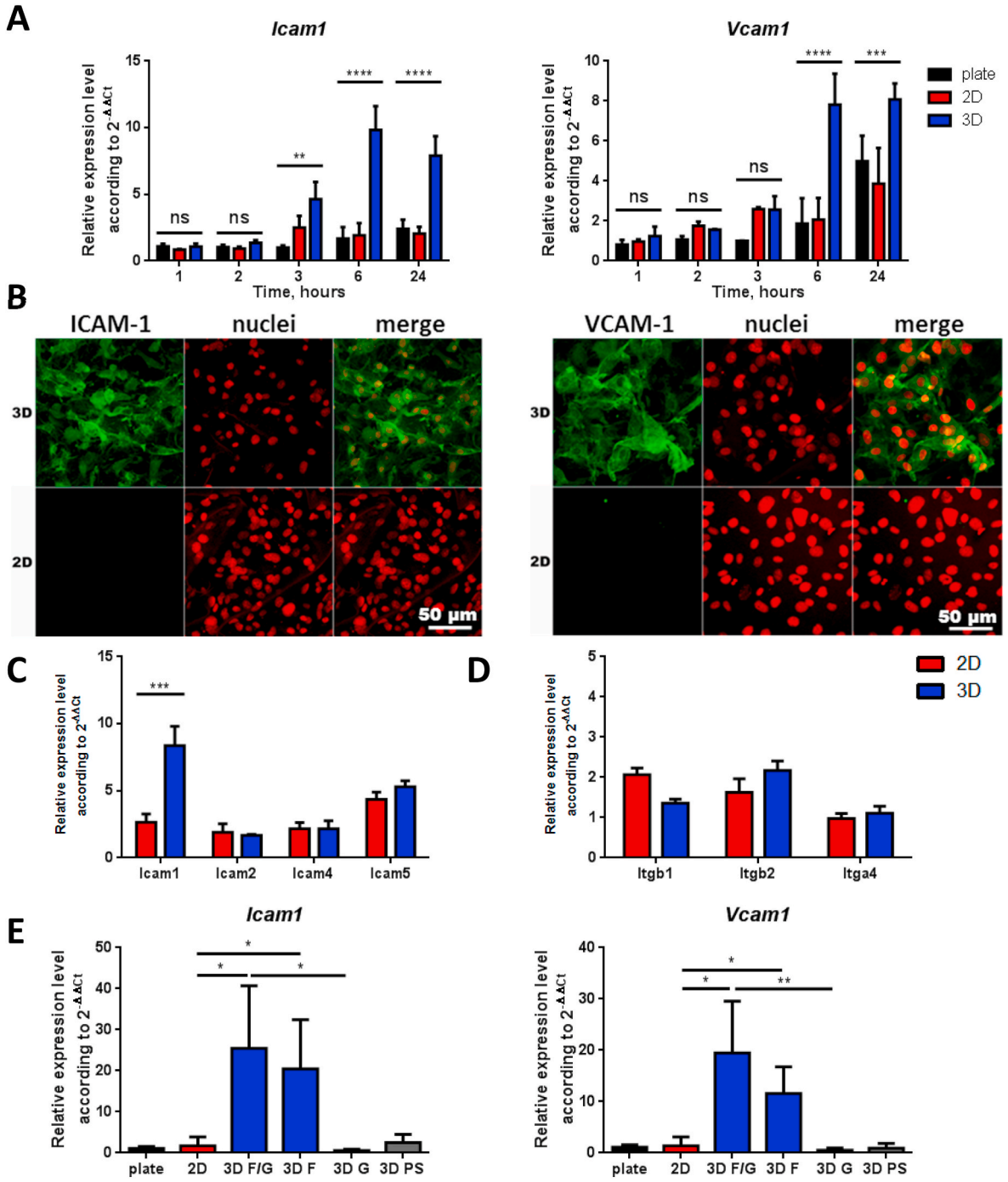

Fig. 1. MEFs, cultured on 3D fibroin/gelatin scaffolds, overexpress adhesion molecules. A –Time-dependent gene expression of *Icam1* and *Vcam1* in MEFs, cultured on control cell culture grade plastic plate, 2D F/G films or in 3D F/G scaffolds (n = 3). **B** – Immunofluorescent staining of ICAM-1 and VCAM-1 (green) on MEFs, cultured on 2D F/G films or in 3D F/G scaffolds for 24 h. Nuclei (red) are stained with SYTOX Orange. **C** – Gene expression of ICAM-family adhesion molecules in MEFs, cultured on 2D F/G films or in 3D F/G scaffolds for 6 h (n = 3). **D** – Gene expression of ICAM-1 and VCAM-1 ligand subunits (*Itgal/Itgb2* and *Itga4/Itgb1*, respectively) in MEFs, cultured on 2D F/G films or in 3D F/G scaffolds for 6 h (n = 3). Expression of *Itgal* was not detected in MEFs. **E** – *Icam1* and *Vcam1* expression in MEFs, cultured for 6 h on control cell culture grade plastic plate, 2D F/G films, 3D F/G, 3D fibroin-only (3D F), 3D gelatin-only (3D G) or 3D polystyrene (3D PS) scaffolds (n = 5). Data from one representative experiment of at least three independent experiments is shown.*p < 0.05, **p < 0.01, ***p < 0.001, ****p < 0.0001, ns – not significant. (For interpretation of the references to colour in this figure legend, the reader is referred to the Web version of this article.)

PBST with 1% skimmed milk and 2% BSA and placed on a shaker for 1 h at +4 °C. Primary antibodies (see Table 2) were added in PBST with skimmed milk and incubated overnight with shaking at +4 °C. After three subsequent washes in PBST (each for 2 h with shaking +4 °C), samples were incubated with secondary antibodies in PBST with skimmed milk overnight with shaking at +4 °C. After three more washing steps, samples were incubated with PBST containing DAPI for 1 h and were imaged using Leica TCS SP5 and Zeiss LSM 510 laser scanning microscopes. Images were analyzed with ImageJ software.

2.10. Immunohistochemistry

Frozen samples of implanted scaffolds were cut using cryotome HM 560 to generate 20 μm sections (ThermoFisher) then placed on glass slides, dried and fixed in cold acetone for 20 min. All subsequent steps were performed in moisture chamber to prevent slides from drying. Samples were washed and permeabilized in TBST (TBS buffer with 0.1% Tween 20) for 5 min. Non-specific binding was blocked by incubation in 5% BSA solution in TBST for 1 h. Next, primary antibodies (see Table 2) in TBST were added for overnight incubation at +4 °C. After three washes in TBST, secondary antibodies were added for 1 h at +4 °C. After final three washes in TBST, slides were mounted with FluoromountG with DAPI (ThermoFisher). Samples were analyzed using Leica TCS SP5 and Zeiss LSM 510 laser scanning microscopes. Images were analyzed with ImageJ software.

2.11. Cytokine production

TNF and IL-6 levels in supernatants collected from the primary MEFs cultures were measured using Mouse TNF-, IL-6, or IL-1β Ready-Set-Go! ELISA Kit (ThermoFisher) according to the manufacturer's instructions.

2.12. Statistical analysis

Data analysis was performed in GraphPad Prism software and presented as mean ± SEM. One-way and two-way ANOVA with Holm-Sidak post-test were used to calculate statistical significance. p-values less than 0.05 were considered to be significant.

3. Results

3.1. Increased expression of ICAM-1 and VCAM-1 in primary MEFs cultured in 3D F/G scaffolds, but not on 2D F/G films

We previously established that fibroin/gelatin scaffolds supplemented with 30% gelatin induce potent growth of primary murine embryonic fibroblasts (MEFs) *in vitro* [30]. However, the impact of the scaffold culture conditions on the phenotype of the stromal cells was not previously investigated. The expression of adhesion molecules is known to be crucial for the function of stromal cells (i.e. fibroblasts), especially, for their contacts and interaction with the immune cells [31,32]. Among the adhesion molecules ICAM-1 and VCAM-1 appear the most relevant, since they mediate lymphocyte adhesion to endothelial cells in the peripheral tissues and lymphoid organs [33–35]. Moreover, ICAM-1/VCAM-1 expression levels correlate with lymph node stromal cell maturation starting with ICAM-1^{-}VCAM-1^{-} lymphoid tissue organizer cells (LToC) differentiating to mature ICAM-1^{hi}VCAM-1^{hi} fibroblastic reticular cells [32]. Thus, we first aimed to determine whether 3D culture conditions on fibroin/gelatin scaffolds may affect the expression of ICAM-1 and VCAM-1 in MEFs.

To investigate the impact of both 3D microenvironment and fibroin/gelatin biomaterial, we setup three types of MEF cultures: a control culture on standard cell culture-grade plastic (control), two-dimensional fibroin/gelatin films (2D F/G) and three-dimensional fibroin/gelatin scaffolds (3D F/G). Interestingly, we found that 3D F/G scaffolds, but not 2D F/G films, induced rapid increase in mRNA expression of both *Icam1* and *Vcam1* genes by MEFs starting as early as 3 h of culture and reaching the peak mRNA level after 6 h (Fig. 1A). This effect was further confirmed at the protein expression level by using immunofluorescence staining after 24 h of incubation (Fig. 1B). Moreover, MEFs maintained upregulated expression profile of *Icam1* and *Vcam1* in 3D F/G scaffold even in 7-day cultures, while in 2D MEF cultures the expression of adhesion molecules remained low even in 3-day cultures, the latest time point analyzed before the cells reached full confluency (Suppl. Fig. 1A). Interestingly, among the ICAM family of adhesion molecules, only ICAM-1 was overexpressed in 3D-cultured MEFs at 6-h time point (Fig. 1C). Expression of the corresponding ligands for ICAM-1 (*Itgal/Itgb2*) and VCAM-1 (*Itga4/Itgb1*) was not affected by 3D culture conditions at 6 h (Fig. 1D). Tissue engineering requires vascularization of implanted scaffolds [36]. To reveal whether culturing of the cells in 3D F/G scaffolds could promote vessel growth upon implantation, expression of VEGF family growth factors, as well as their receptor subunits was analyzed in plate- and 3D-cultured MEFs. Significant upregulation of *Vegfa*, *Vegfb*, and *Vegfc* was observed, while only Flt1 receptor subunit demonstated increased expression in 3D culture system (Suppl. Fig. 1B). These data indicate that 3D F/G scaffolds could possibly promote vascularization upon implantation *in vivo*.

Previous studies on human monocytes suggested that the effects of 3D fibroin scaffolds may be due to specific changes in fibroin conformation in these scaffolds, rather than to 3D microenvironment *per se* [20]. To address this possibility, we performed additional experiments using commercially available 3D polystyrene scaffolds (3D PS) as 3D microenvironment control. Indeed, 3D PS-cultured MEFs failed to show an increase in ICAM-1 and VCAM-1 expression, suggesting that this effect was specific to 3D F/G scaffolds (Fig. 1E). Finally, since collagen and its derivatives can potentially alter expression of adhesion molecules by the cells [37], we analyzed MEFs cultured on 3D fibroin-only scaffolds and found the same upregulation of ICAM-1/VCAM-1 expression, suggesting that this effect was not related to gelatin moiety in the scaffolds (Fig. 1E), but rather was induced by specific properties of 3D fibroin itself. In line with this, no upregulation of *Icam1* and *Vcam1* was observed in MEFs cultured on 3D gelatin-only scaffolds (3D G, Fig. 1E). Together our data indicate that 3D F/G scaffolds in contrast to 2D F/G films promote overexpression of adhesion molecules ICAM-1 and VCAM-1 in primary MEF cultures.

3.2. TNF is partially responsible for Icam1 and Vcam1 overexpression in MEFs cultured in 3D F/G scaffolds

We next investigated the mechanism driving the overexpression of adhesion molecules in 3D-cultured MEFs. First, we asked if this effect required any soluble mediators, produced by cells in response to 3D scaffolds, which induced the overexpression of adhesion molecules in autocrine manner. To test this hypothesis, we performed experiments with the transfer of conditioned medium from control, 2D- or 3D F/G-cultured MEFs to MEFs that were cultured in standard conditions (Fig. 2A). Strikingly, we observed a significant increase in expression of *Icam1* and *Vcam1* only in those MEFs that received conditioned medium from 3D F/G-cultured MEFs (Fig. 2B). Importantly, using conditioned medium from different time points, we observed clear time dynamics in the expression of adhesion molecules. Medium from MEFs cultured in 3D scaffolds for 2–3 h failed to induce significant expression of *Icam1* and *Vcam1*. However, medium from MEFs cultured in 3D scaffolds for 6 or 24 h induced significant upregulation of *Icam1* expression by MEFs, cultured under standard conditions (10-15-fold increase as compared to control cells). At the same time, moderate increase in *Vcam1* expression was observed when using medium from MEFs, cultured in 3D scaffolds for 24 h (3-5-fold increase as compared to control cells). Thus, our data indicate that *Icam1* and *Vcam1* expression in 3D-cultured MEFs was induced by soluble mediators.

Various cytokines and stress factors are known to induce ICAM-1/VCAM-1 expression in fibroblasts [38–40]. Since F/G microparticles

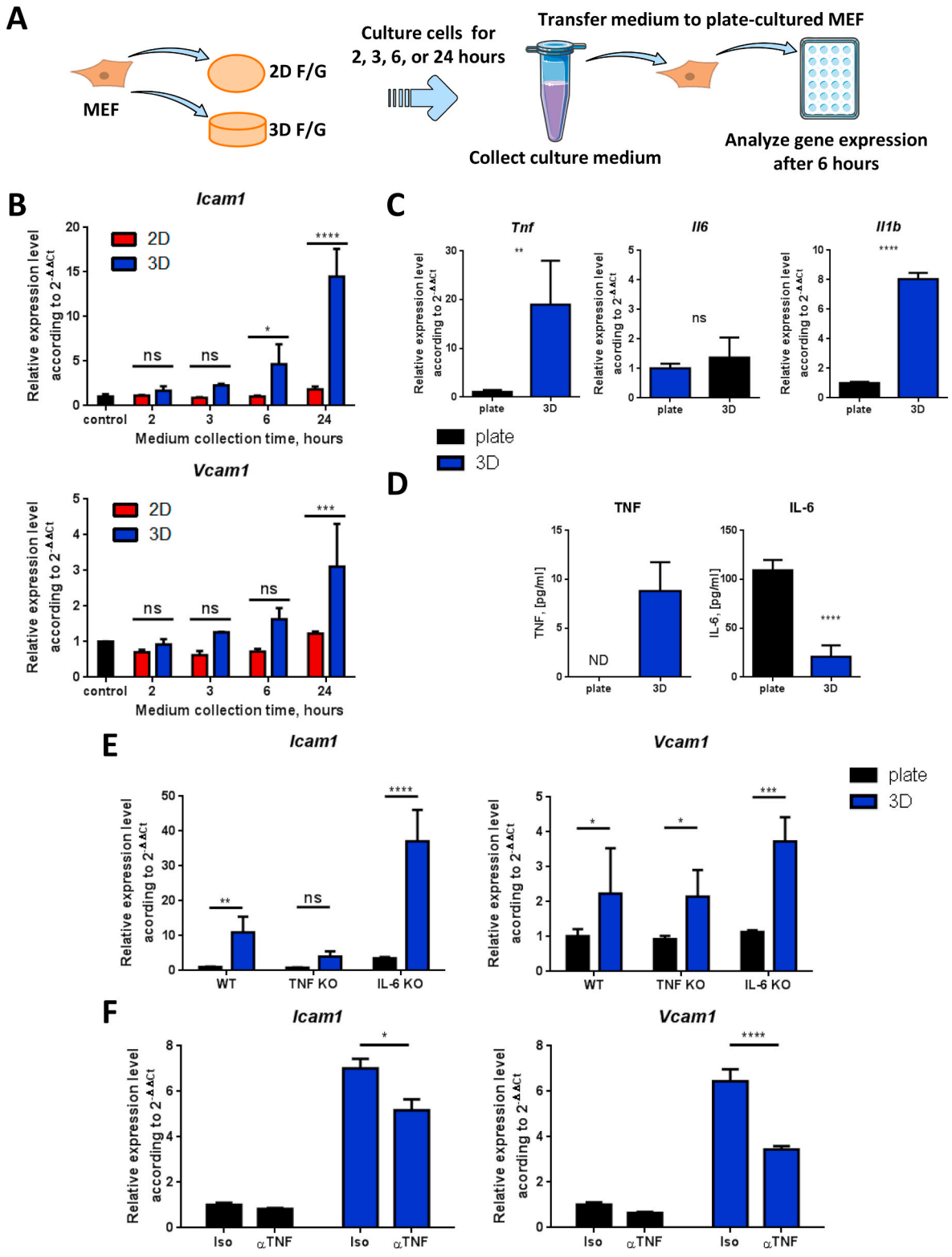

Fig. 2. MEFs, cultured on 3D fibroin/gelatin scaffolds, produce TNF and downregulate production of IL-6. **A** – Schematic design of conditioned medium transfer experiment. **B** – Expression of *Icam1* and *Vcam1* in MEFs, cultured on plate for 6 h following transfer of conditioned medium from MEFs, cultured on 2D F/G films or in 3D F/G scaffolds, for indicated timepoint (2–24 h) (n = 3). **C** – Expression of *Tnf, Il6,* and *Il1b* genes in MEFs, cultured on control cell culture grade plastic plate or in 3D F/G scaffolds (n = 4). **D** – TNF and IL-6 proteins in culture medium of plate- or 3D F/G-cultured MEFs (n = 4). IL-1β was not detected in analyzed samples. **E** – *Icam1* and *Vcam1* expression in TNF KO and IL-6 KO MEFs, cultured on cell culture grade plastic plate or in 3D F/G scaffolds (n = 3). Data are relative to expression level in plate-cultured WT MEFs. **F** – *Icam1* and *Vcam1* expression in MEFs cultured on cell culture grade plastic plate or in 3D F/G scaffolds in the presence of neutralizing anti-TNF antibody (αTNF) or isotype control (Iso) (n = 3). Data are relative to expression level in plate-cultured MEFs with isotype control antibody. Gene expression was analyzed after 6 h of culturing cells in above mentioned conditions. Data from one representative experiment of the two independent experiments is shown. *p < 0.05, **p < 0.01, ***p < 0.001, ****p < 0.0001, ns – not significant.

have been previously characterized to induce moderate inflammatory response [21], we evaluated the expression of the three most prominent proinflammatory cytokines, known to induce ICAM-1 and VCAM-1 expression: TNF, IL-6, and IL-1β [41–43], and, surprisingly, found that only TNF was expressed in 3D F/G-cultured MEFs both at mRNA (Fig. 2C) and at protein level (Fig. 2D). Moreover, MEFs from TNF KO mice failed to overexpress *Icam1* in 3D culture conditions (Fig. 2E), while *Vcam1* expression was not affected. Strikingly, IL-6 KO MEFs demonstrated increased *Icam1* expression at steady state, indicating that IL-6 is rather involved in downregulation of *Icam1* (Suppl. Fig. 2A). Finally, the role of TNF in upregulation of adhesion molecules was confirmed by using neutralizing anti-TNF antibody, which significantly suppressed both *Icam1* and *Vcam1* expression in 3D-cultured MEFs (Fig. 2F). Altogether, our data demonstrate that upregulation of *Icam1* and *Vcam1* expression by MEFs cultured in 3D F/G scaffolds was driven by soluble TNF.

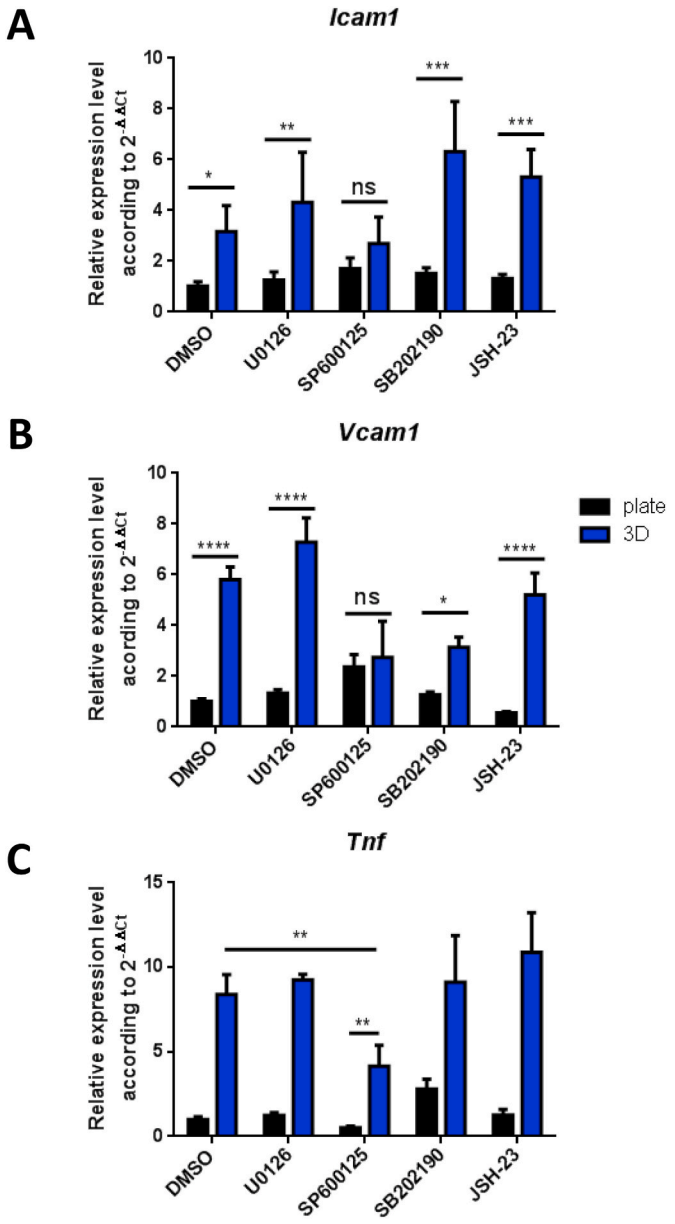

Fig. 3. ICAM-1 and VCAM-1 overexpression in 3D F/G-cultured MEFs is mediated by JNK. Gene expression of *Icam1* (**A**), *Vcam1* (**B**) and *Tnf* (**C**) in MEFs, cultured on control cell culture grade plastic plate or in 3D F/G scaffolds in the presence of DMSO or inhibitors of ERK1/2 (U0126), JNK1/2 (SP600125), p38 (SB202190) or classical NFκB (JSH-23) (n = 3). Gene expression was analyzed after 6 h of culturing cells in above mentioned conditions. Data are relative to DMSO-treated plate-cultured MEFs. Data from one representative experiment of at least three independent experiments is shown. *p < 0.05, **p < 0.01, ***p < 0.001, ****p < 0.0001, ns – not significant.

3.3. Expression of adhesion molecules in MEFs cultured in 3D F/G scaffolds is mediated by JNK

Next, we aimed to assess the intracellular pathways responsible for adhesion molecule upregulation by MEFs, cultured in 3D F/G scaffolds. In order to do so, we performed experiments with selective inhibitors of key MAP kinases (ERK1/2, JNK1/2, p38), as well as a classical NFκB inhibitor. We found that selective inhibition of JNK resulted in abrogated *Icam1* and *Vcam1* expression in 3D F/G-cultured MEFs (Fig. 3A and B). In addition, *Tnf* expression was also reduced after inhibition of JNK (Fig. 3C), suggesting that activation of this kinase controls TNF expression by MEFs. Taken together, our data indicate that in MEFs cultured in 3D F/G scaffolds JNK mediates the expression of TNF, which, in turn, induces the expression of ICAM-1 and VCAM-1.

3.4. MEFs with overexpressed ICAM-1/VCAM-1 promote lymphocyte adhesion and retention in 3D F/G scaffolds in vitro

ICAM-1 and VCAM-1 are important for lymphocyte adhesion during inflammatory responses [33,34], as well as during homeostatic recirculation through lymphoid tissues [35]. Thus, we hypothesized that overexpression of ICAM-1/VCAM-1 in 3D F/G-cultured MEFs may promote their interaction with immune cells and can potentially be used for artificial lymphoid tissue engineering. To test this idea *in vitro,* we performed co-culture assays in which we first established GFP^+ MEFs culture on 2D F/G-coated glass surface or in 3D F/G scaffolds and then added $CD4^+$ splenocytes, enriched for T lymphocytes (Suppl. Fig. 2B). The number of $CD4^+$ cells which became adherent to MEFs after 4 h of co-culture was calculated for each culture condition using immunofluorescent staining and confocal microscopy (Fig. 4A). We found that only 3D F/G-cultured MEFs promoted sufficient $CD4^+$ T cell adhesion (Fig. 4B) and observed clusters of lymphocytes, attached to MEFs in 3D F/G scaffolds (Fig. 4A). To verify that this interaction was mediated by adhesion molecules, we used monoclonal antibodies to block ICAM-1 or VCAM-1. We found that both antibodies could disrupt lymphocyte adhesion to MEFs in 3D F/G scaffolds (Fig. 4B), suggesting that both ICAM-1 and VCAM-1 are crucial for MEF-$CD4^+$ lymphocyte interaction. Altogether, we demonstrated that 3D F/G-induced overexpression of adhesion molecules by MEFs is required for cell-to-cell interactions with $CD4^+$ T lymphocytes *in vitro* and supports lymphocyte retention in the scaffold.

3.5. Implantation of 3D F/G scaffolds induces infiltration and clustering of lymphocytes in vivo

We established that 3D fibroin/gelatin scaffolds induced the activation of fibroblasts (i.e. MEFs) resulting in upregulation of adhesion molecules ICAM-1/VCAM-1 and increased adhesion of $CD4^+$ T lymphocytes to MEFs. Our final goal was to determine whether this effect of 3D F/G scaffolds can influence their functional properties *in vivo*. The regenerative potential of these scaffolds was previously validated in tissue regeneration models [21,44,45]. However, the interaction of this biomaterial with the immune cells *in vivo* was not previously addressed. To investigate the interplay between immune system and 3D F/G scaffolds *in vivo*, we implanted the matrices under the kidney capsule of mice and analyzed the composition and distribution of immune cells in the implants after 3 weeks using immunohistochemistry. For controls we used well-described commercially available collagen scaffolds of comparable size which do not induce robust immune cell infiltration without additional stimulation [46].

Three weeks after transplantation both types of scaffolds were

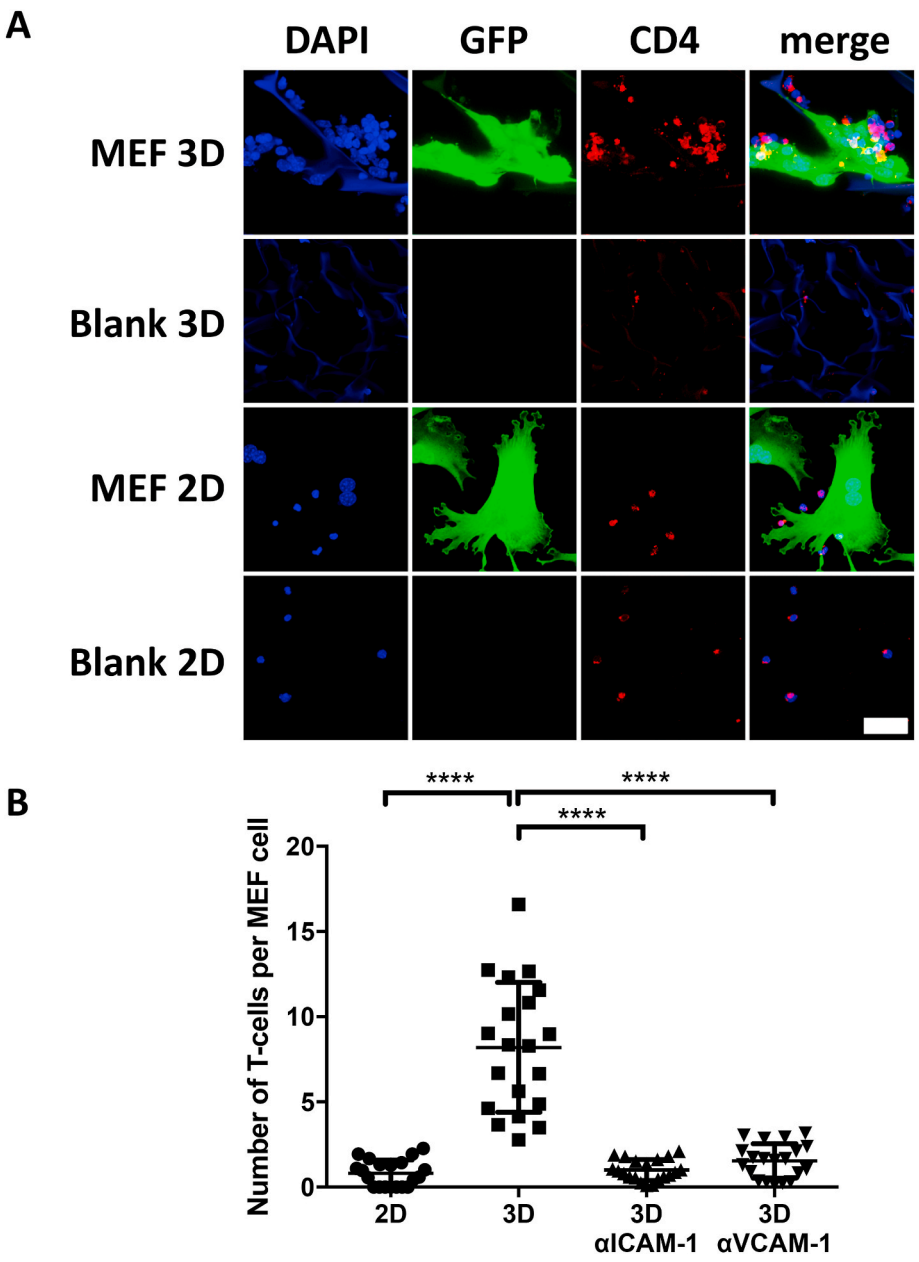

Fig. 4. MEFs, cultured in 3D F/G scaffolds, support ICAM-1/VCAM-1-dependent adhesion of CD4$^+$ lymphocytes. **A** – Representative microphotographs of CD4$^+$ cells (red) cultured with GFP$^+$ MEFs (green) on 2D F/G-coated glass or in 3D F/G scaffolds. Nuclei (blue) are stained with DAPI. Scale bar 25 μm. **B** – Calculated number of CD4$^+$ cells attached to one fibroblast (combined data from 3 scaffolds, 5 view fields each). MEFs were cultured on 2D F/G-coated glass or in 3D F/G scaffolds. Additionally, in 3D conditions inhibition of ICAM-1 or VCAM-1 was carried out using blocking antibodies (αICAM-1 and αVCAM-1, respectively). Data from one representative experiment of at least three independent experiments is shown. ****$p < 0.0001$. (For interpretation of the references to colour in this figure legend, the reader is referred to the Web version of this article.)

sufficiently vascularized as revealed by CD31 immunostaining (Fig. 5A). Strikingly, only 3D F/G scaffolds induced significant infiltration of CD4$^+$ T cells (Fig. 5B) and B220$^+$ B cells upon implantation (Fig. 5C). Moreover, B cells in implanted 3D F/G scaffolds were clustered into primitive lymphoid follicles (Fig. 5E), while T cells were mainly distributed between such B cell clusters (Suppl. Fig. 3A). In contrast, no significant infiltration and/or clustering of lymphocytes were found in implanted collagen scaffolds as compared to F/G implants (Fig. 5E). Small numbers of B cells in implanted collagen scaffolds can possibly be explained by lower expression of B cell attracting chemokine *Cxcl13* (Suppl. Fig. 3B). No other markers for mature lymphoid tissues (e.g. FDC-M1, PNAd, MAdCAM-1) were expressed by the cells in the implants (data not shown). At the same time, no difference in macrophage infiltration between the two types of scaffolds was observed (Fig. 5D). Altogether, our data suggested that 3D fibroin/gelatin scaffolds induce specific infiltration and clustering of adaptive immune cells upon implantation under the kidney capsule *in vivo*.

4. Discussion

Biomaterials are attracting a lot of attention due to potentially wide range of applications in translational medicine, including targeted drug delivery, regeneration or replacement of damaged tissue, bioengineering of artificial organs for transplantation, generation of surgical suture materials and others. In most cases, biomaterials are expected to behave as inert scaffolds or vehicles that lack their own biological activity and are either resorbed or excreted from the organism after some time. The important feature for biomaterials is their biocompatibility that includes lack of toxicity, pyrogenicity, and, at the same time, ability to support cell adhesion and growth that are crucial for regeneration and tissue engineering [47,48]. However, in addition to biocompatibility, some artificial materials can unexpectedly affect the surrounding cells and induce certain transcriptional and translational changes, which should be taken into account before such materials can be applied to clinical setting [49,50].

Among natural biopolymers used for scaffolding materials, the silk

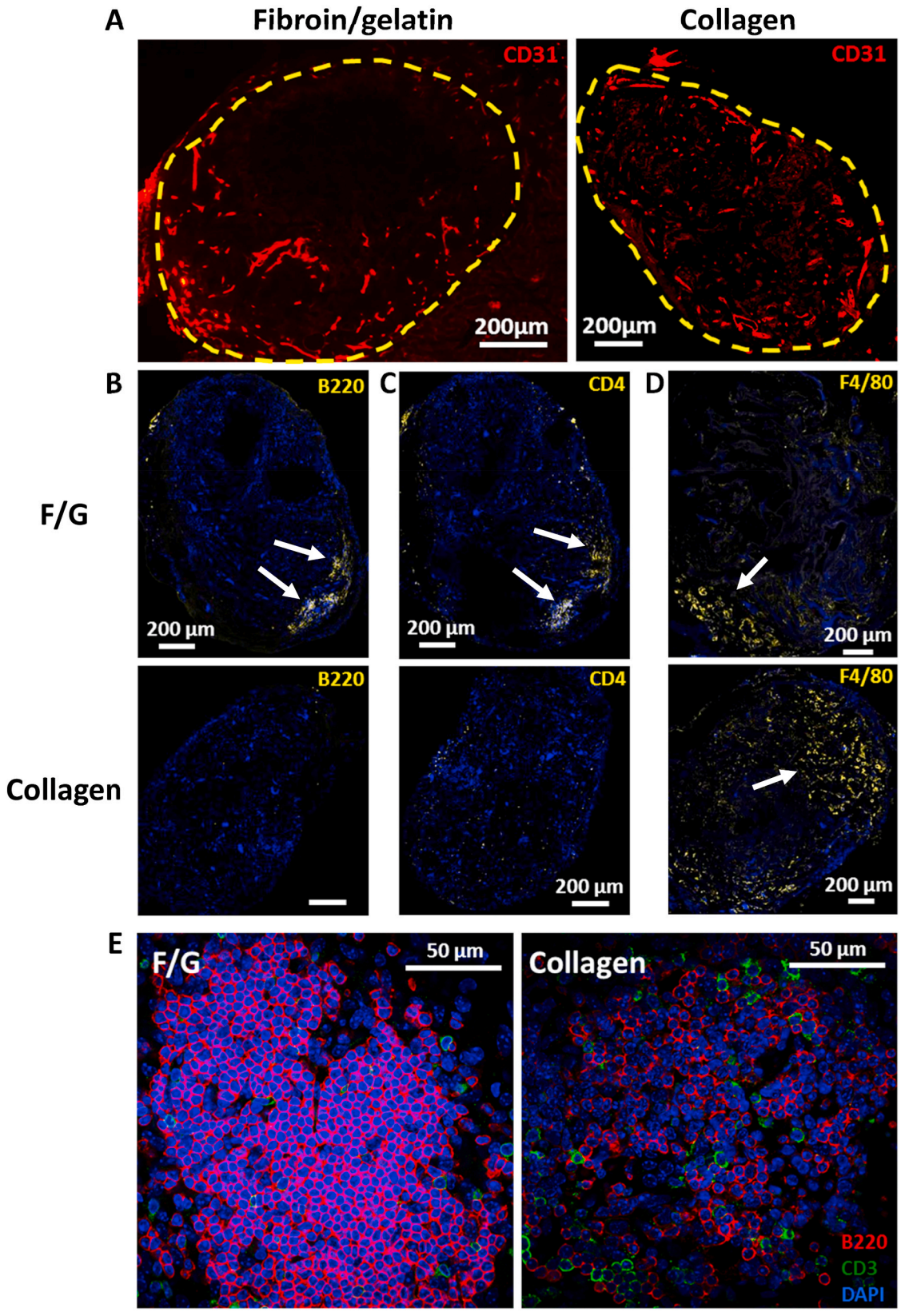

Fig. 5. Implantation of F/G, but not collagen scaffolds, results in infiltration and clustering of lymphocytes *in vivo*. **A** – CD31 (red) immunohistochemistry staining of implanted 3D F/G or collagen scaffolds 3 weeks after implantation. Dotted yellow line indicates the border of the implant. Immunohistochemistry staining (yellow) for B220 (**B**), CD4 (**C**) and F4/80 (**D**) of implanted 3D F/G or collagen scaffolds 3 weeks after implantation. Nuclei (blue) are stained with DAPI. White arrows indicate clusters of T- and B-cells in 3D F/G implanted scaffolds, as well as clusters of macrophages in both types of implanted scaffolds. **E** – Immunofluorescent staining for B220 (red), CD3 (green) and DAPI (blue) of implanted 3D F/G or collagen scaffolds 3 weeks after implantation. Scanning was performed from the surface of the implant. Data from one representative experiment of at least three independent experiments is shown. (For interpretation of the references to colour in this figure legend, the reader is referred to the Web version of this article.)

proteins show several unique features that make them valuable for tissue engineering [51–54]. First, silk-based biomaterials demonstrate extremely high mechanical strength with, for example, dragline silk being five times stronger by weight than steel [55]. At the same time, silk polymers are characterized by high elasticity and increased resistance to compression as compared to other high performance fibers [51]. Silk is used to fabricate scaffolds in various forms, including 2D films, 3D sponges, hydrogels, micro- and nanoparticles, fibers. Several modifications of silk-based scaffolds have been described [30,56,57]. Among them modification with gelatin, a mixture of type I collagen partial hydrolysis products, was introduced to improve biocompatibility, as well as physical and chemical properties of silk fibroin scaffolds [23,58]. Importantly, gelatin modification introduces RGD (Arg-Gly-Asp tripeptide) sequences to the silk-based scaffolds [58], thus, improving cell adhesion, migration, and proliferation of cells on fibroin/gelatin (F/G) biomaterial as compared to pure fibroin (F), lacking RGD sequence. These properties of fibroin/gelatin scaffolds are useful for generating 3D scaffolds for tissue engineering and regenerative medicine. For example, fibroin/gelatin blends were recently employed for generation of bioinks, suitable for 3D printing of soft tissue implants [59].

In present study we uncovered novel biological effects of previously characterized biocompatible silk fibroin-based scaffolds both *in vitro* and *in vivo*. First, we found that three-dimensional (3D) fibroin or fibroin/gelatin scaffolds may induce rapid expression of adhesion molecules ICAM-1 and VCAM-1 in the primary culture of mouse embryonic fibroblasts (Fig. 1). Surprisingly, two-dimensional (2D) composition of fibroin/gelatin scaffolds (either as films or glass coating) did not induce significant changes in gene expression by MEFs. This data is in line with previously published report on the effect of 3D, but not 2D, fibroin scaffolds on human monocytes [20]. However, MEFs acquired changes in their expression program that were different from monocytes with decreased expression of IL-6 and increased expression of TNF and adhesion molecules (Figs. 1 and 2), suggesting a distinct type of effects of fibroin-based 3D scaffolds on different cell types. Intracellular signaling pathways responsible for these effects also appear to differ in MEFs as compared to human monocytes. Importantly, we found that inhibition of JNK can specifically suppress 3D F/G-mediated upregulation of ICAM-1/VCAM-1 in MEFs. Recently, activation of the classical NFκB by monomeric silk fibroin was detected in murine and human fibroblasts [60]. However, in our hands, inhibition of the classical NFκB did not affect the expression of adhesion molecules by MEFs, thus, supporting the idea that the effect of 3D F/G scaffolds is not mediated by cleaved soluble fibroin. At the same time, our data indicate that TNF is partially responsible for ICAM-1 and VCAM-1 expression in MEFs cultured in 3D F/G scaffolds, suggesting that other signaling pathways (including, possibly, JNK) apart from the classical NFκB may mediate this effect of TNF. Interestingly, the effect of macroscopic 3D scaffolds differs from 3D F/G microparticles, which induce expression of both TNF and IL-6 by MEFs, as recently reported [21]. Possibly, this reflects the differences in microenvironment in these two types of biomaterials, for example, reduced diffusion of oxygen in macroscopic 3D scaffolds as compared to microscopic particles.

Of note, one cannot completely rule out possible effects on cells and on gene expression of such physical properties as the pore size or the stiffness of bioengineered materials. There is evidence that cells cultured on stiff surface may alter the expression of ICAM-1 and VCAM-1 [61]. Physical and chemical properties of 2D F/G films and 3D F/G scaffolds used in this study were previously described [62]. The pore size of 3D scaffolds comprised of different materials used in this study was comparable, ranging from 200 μm in diameter for 3D polystyrene scaffolds to 220 ± 65 μm and 250 ± 80 μm for fibroin and fibroin/gelatin scaffolds, respectively. At the same time, the mechanical stiffness was different for the type of materials used, among which the most rigid was 3D polystyrene with shear modulus ~ 3×10^6 kPa [63], compared to 9.0 ± 1.6 kPa for fibroin/gelatin and at 5.9 ± 1.1 kPa for fibroin. Nevertheless, these differences in rigidness between fibroin and F/G-scaffolds did not significantly affect expression of adhesion molecules, since ICAM-1 expression was highly upregulated in both types of scaffolds, suggesting a stronger contribution from the fibroin itself, rather than from the differences in physical properties of bioengineered materials.

Adhesion molecules are important for stromal cell functions and are involved in their interactions with immunocytes [31,64]. In embryonic lymph node development, expression of ICAM-1 and VCAM-1 is significantly increased during the process of lymph node stromal cell maturation, reflecting the growing influx of lymphocytes into lymphoid sacs [32]. In line with this, we observed a drastic increase in adhesion of $CD4^+$ cells to MEFs cultured in 3D F/G scaffolds, but not in those cultured under conventional 2D conditions (Fig. 4). Since inhibition of ICAM-1 and VCAM-1 with specific antibodies abrogated $CD4^+$ cell attachment to MEFs, we concluded that this interaction was indeed ICAM-1/VCAM-1-dependent. Thus, our data strongly suggest that 3D F/G scaffolds can induce functional changes in stromal cells, which may affect their interactions with the immune cells. This property might be beneficial for generation of scaffold-based vaccines, for example, in the highly relevant field of tumor therapy [4,5]. One may expect that F/G scaffolds will be superior in attracting T lymphocytes and, thus, promoting antigen-specific immune responses as compared to other biomaterials, lacking the ability to rapidly induce and sustain the expression of adhesion molecules by stromal cells.

Of particular significance, our *in vivo* data suggested that F/G scaffolds promote infiltration and clustering of lymphocytes (Fig. 5, Suppl. Fig. 3). The fact that implanted scaffolds become well vascularized (Fig. 5A) suggests that they are not rejected upon implantation. Furthermore, 3D F/G scaffolds could promote expression of VEGF growth factors (Suppl. Fig. 1B) in fibroblasts, potentially promoting vessels growth. Interestingly, T cells and B cells in implanted F/G scaffolds acquired zonal distribution, similar to those observed in the secondary and tertiary lymphoid organs, although no markers specific for mature lymphoid tissue were upregulated in the implanted scaffolds (data not shown). Migration of immune cell requires the presence of chemokines that stimulate cell egress into the tissues and guide different cell types to their niches, maintaining zonal distribution of cells within the organ [65]. In lymphoid tissues CCL19 and CCL21 mainly govern migration of T cells to T-zones, while CXCL13 attracts B cells to the follicles [66]. Surprisingly, implanted F/G scaffolds induced significant expression of *Cxcl13* (Suppl. Fig. 3B), that, presumably, drove B cell infiltration and clustering (Fig. 5B). At the same time, implanted collagen scaffolds showed reduced *Cxcl13* expression and, consequently, contained a smaller number of B cells (Fig. 5B). Thus, upon implantation F/G scaffolds may induce the expression of lymphoid tissue-specific chemokine *Cxcl13* and stimulate infiltration of lymphocytes. This feature can be employed for generating artificial lymphoid tissues that represent another potential therapeutic tool for vaccinations [67–70]. Our findings suggest that F/G scaffolds can provide suitable microenvironment for construction of such organs since they can promote lymphocyte infiltration, adhesion and proper initial clustering, which can be further guided and manipulated by specific chemokine and cytokine signaling. Altogether, our data uncover novel biological properties of 3D fibroin/gelatin scaffolds *in vitro* and *in vivo* which affect stromal cell phenotype and promote lymphocyte infiltration and adhesion inside the scaffolds.

CRediT authorship contribution statement

Maxim A. Nosenko: Conceptualization, Methodology, Investigation, Formal analysis, Visualization, Writing. **Anastasia M. Moysenovich:** Methodology, Investigation, Writing, Visualization, Resources. **Anastasia Y. Arkhipova:** Investigation. **Kamar-Sulu N. Atretkhany:** Investigation. **Sergei A. Nedospasov:** Conceptualization, Writing, Funding acquisition. **Marina S. Drutskaya:** Conceptualization,

Supervision, Project administration, Writing, Funding acquisition. **Mikhail M. Moisenovich:** Conceptualization, Methodology, Supervision, Project administration, Writing, Funding acquisition, Visualization, Resources.

Declaration of competing interest

The authors declare that they have no known competing financial interests or personal relationships that could have appeared to influence the work reported in this paper.

Acknowledgements

We thank Drs. Nadezhda Logunova and Andrey Kruglov for providing critical materials. This work was supported by the Russian Science Foundation grant #19-75-30032. Genotyping of mice and primary cell cultures was supported by grant 075-15-2019-1660 from the Ministry of Science and Higher Education of the Russian Federation. Generation of TNF KO and IL-6 KO MEFs was supported by the Russian Foundation for Basic Research grant #19-04-01094.

Dedicated to the memory of Dr. Mikhail Moisenovich.

Appendix A. Supplementary data

Supplementary data related to this article can be found at https://doi.org/10.1016/j.bioactmat.2021.03.016.

References

[1] G. Gainza, S. Villullas, J.L. Pedraz, R.M. Hernandez, M. Igartua, Advances in drug delivery systems (DDSs) to release growth factors for wound healing and skin regeneration, Nanomed. Nanotechnol. Biol. Med. 11 (2015) 1551–1573, https://doi.org/10.1016/j.nano.2015.03.002.

[2] A. Singh, Biomaterials innovation for next generation ex vivo immune tissue engineering, Biomaterials 130 (2017) 104–110, https://doi.org/10.1016/j.biomaterials.2017.03.015.

[3] T. Nardo, I. Carmagnola, F. Ruini, S. Caddeo, S. Calzone, V. Chiono, G. Ciardelli, Synthetic biomaterial for regenerative medicine applications, in: Kidney Transplantation, Bioeng. Regen., Elsevier, 2017, pp. 901–921, https://doi.org/10.1016/B978-0-12-801734-0.00065-5.

[4] O.A. Ali, N. Huebsch, L. Cao, G. Dranoff, D.J. Mooney, Infection-mimicking materials to program dendritic cells in situ, Nat. Mater. 8 (2009) 151–158, https://doi.org/10.1038/nmat2357.Infection-Mimicking.

[5] J. Kim, W.A. Li, Y. Choi, S.A. Lewin, C.S. Verbeke, G. Dranoff, D.J. Mooney, Injectable, spontaneously assembling, inorganic scaffolds modulate immune cells in vivo and increase vaccine efficacy, Nat. Biotechnol. 33 (2015) 64–72, https://doi.org/10.1038/nbt.3071.

[6] N. Okamoto, R. Chihara, C. Shimizu, S. Nishimoto, T. Watanabe, Artificial lymph nodes induce potent secondary immune responses in naive and immunodeficient mice, J. Clin. Invest. 117 (2007) 997–1007, https://doi.org/10.1172/JCI30379.utes.

[7] C.M. Nelson, M.J. Bissell, Of extracellular matrix, scaffolds, and signaling: tissue architecture regulates development, homeostasis, and cancer, Annu. Rev. Cell Dev. Biol. 22 (2006) 287–309, https://doi.org/10.1146/annurev.cellbio.22.010305.104315.

[8] M.P. Lutolf, J.A. Hubbell, Synthetic biomaterials as instructive extracellular microenvironments for morphogenesis in tissue engineering, Nat. Biotechnol. 23 (2005) 47–55, https://doi.org/10.1038/nbt1055.

[9] L.G. Griffith, Emerging design principles in biomaterials and scaffolds for tissue engineering, Ann. N. Y. Acad. Sci. 961 (2002) 83–95, https://doi.org/10.1111/j.1749-6632.2002.tb03056.x.

[10] M.A. Nosenko, M.S. Drutskaya, M.M. Moisenovich, S.A. Nedospasov, Bioengineering of artificial lymphoid organs, Acta Naturae 8 (2016) 10–23.

[11] S. Samavedi, L.K. Poindexter, M. Van Dyke, A.S. Goldstein, Synthetic biomaterials for regenerative medicine applications. Regen. Med. Appl. Organ Transplant., Elsevier, 2014, pp. 81–99, https://doi.org/10.1016/B978-0-12-398523-1.00007-0.

[12] V.A. Zhuikov, Y.V. Zhuikova, T.K. Makhina, V.L. Myshkina, A. Rusakov, A. Useinov, V.V. Voinova, G.A. Bonartseva, A.A. Berlin, A.P. Bonartsev, A. L. Iordanskii, Comparative structure-property characterization of poly(3-hydroxybutyrate-Co-3-Hydroxyvalerate)s films under hydrolytic and enzymatic degradation: finding a transition point in 3-hydroxyvalerate content, Polymers 12 (2020) 728, https://doi.org/10.3390/polym12030728.

[13] D.M. Faulk, S.F. Badylak, V. Chiono, T. Nardo, G. Ciardelli, D.M. Faulk, S. F. Badylak, Natural biomaterials for regenerative medicine applications. Regen. Med. Appl. Organ Transplant., Elsevier, 2014, pp. 101–112, https://doi.org/10.1016/B978-0-12-398523-1.00009-4.

[14] J.L. Drury, D.J. Mooney, Hydrogels for tissue engineering: scaffold design variables and applications, Biomaterials 24 (2003) 4337–4351, https://doi.org/10.1016/S0142-9612(03)00340-5.

[15] J.M. Aamodt, D.W. Grainger, Extracellular matrix-based biomaterial scaffolds and the host response, Biomaterials 86 (2016) 68–82, https://doi.org/10.1016/j.biomaterials.2016.02.003.

[16] E. Santos-Vizcaino, A. Salvador, C. Vairo, M. Igartua, R.M. Hernandez, L. Correa, S. Villullas, G. Gainza, Overcoming the inflammatory stage of non-healing wounds: in vitro mechanism of action of negatively charged microspheres (NCMS), Nanomaterials 10 (2020) 1–14, https://doi.org/10.3390/nano10061108.

[17] F. Chogan, T. Mirmajidi, A.H. Rezayan, A.M. Sharifi, A. Ghahary, J. Nourmohammadi, A. Kamali, M. Rahaie, Design, fabrication, and optimization of a dual function three-layer scaffold for controlled release of metformin hydrochloride to alleviate fibrosis and accelerate wound healing, Acta Biomater. 113 (2020) 144–163, https://doi.org/10.1016/j.actbio.2020.06.031.

[18] U. Ripamonti, L.C. Roden, L.F. Renton, Osteoinductive hydroxyapatite-coated titanium implants, Biomaterials 33 (2012) 3813–3823, https://doi.org/10.1016/j.biomaterials.2012.01.050.

[19] H. Liu, J. Lin, K. Roy, Effect of 3D scaffold and dynamic culture condition on the global gene expression profile of mouse embryonic stem cells, Biomaterials 27 (2006) 5978–5989, https://doi.org/10.1016/j.biomaterials.2006.05.053.

[20] M. Bhattacharjee, E. Schultz-Thater, E. Trella, S. Miot, S. Das, M. Loparic, A.R. Ray, I. Martin, G.C. Spagnoli, S. Ghosh, The role of 3D structure and protein conformation on the innate andadaptive immune responses to silk-based biomaterials, Biomaterials 34 (2013) 8161–8171, https://doi.org/10.1016/j.biomaterials.2013.07.018.

[21] M.A. Nosenko, A.M. Moysenovich, R. V Zvartsev, A.Y. Arkhipova, A.S. Zhdanova, I. I. Agapov, T. V Vasilieva, V.G. Bogush, V.G. Debabov, S. Nedospasov, M. M. Moisenovich, M.S. Drutskaya, Novel biodegradable polymeric microparticles facilitate scarless wound healing by promoting re-epithelialization and inhibiting fibrosis, Front. Immunol. 9 (2018) 2851, https://doi.org/10.3389/FIMMU.2018.02851.

[22] M.A. Nosenko, N.V. Maluchenko, M.S. Drutskaya, A.Y. Arkhipova, I.I. Agapov, S. A. Nedospasov, M.M. Moisenovich, Induction of ICAM-1 expression in mouse embryonic fibroblasts cultured on fibroin-gelatin scaffolds, Acta Naturae 9 (2017) 89–93.

[23] A.A. Orlova, M.S. Kotlyarova, V.S. Lavrenov, S.V. Volkova, A.Y. Arkhipova, Relationship between gelatin concentrations in silk fibroin-based composite scaffolds and adhesion and proliferation of mouse embryo fibroblasts, Bull. Exp. Biol. Med. 158 (2014) 88–91, https://doi.org/10.1007/s10517-014-2699-2.

[24] D. V Kuprash, A. V Tumanov, D.J. Liepinsh, E.P. Koroleva, M.S. Drutskaya, A. A. Kruglov, A.N. Shakhov, E. Southon, W.J. Murphy, L. Tessarollo, S. I. Grivennikov, S.A. Nedospasov, Novel tumor necrosis factor-knockout mice that lack Peyer's patches, Eur. J. Immunol. 35 (2005) 1592–1600, https://doi.org/10.1002/eji.200526119.

[25] A. Quintana, M. Erta, B. Ferrer, G. Comes, M. Giralt, J. Hidalgo, Astrocyte-specific deficiency of interleukin-6 and its receptor reveal specific roles in survival, body weight and behavior, Brain Behav. Immun. 27 (2013) 162–173, https://doi.org/10.1016/j.bbi.2012.10.011.

[26] D.A. Conner, Mouse embryo fibroblast (MEF) feeder cell preparation, Curr. Protoc. Mol. Biol. 23 (2001) 1–7, https://doi.org/10.1002/0471142727.mb2302s51.

[27] J. Schindelin, I. Arganda-Carreras, E. Frise, V. Kaynig, M. Longair, T. Pietzsch, S. Preibisch, C. Rueden, S. Saalfeld, B. Schmid, J.-Y. Tinevez, D.J. White, V. Hartenstein, K. Eliceiri, P. Tomancak, A. Cardona, Fiji: an open-source platform for biological-image analysis, Nat. Methods 9 (2012) 676–682, https://doi.org/10.1038/nmeth.2019.

[28] L.D. Shultz, N. Goodwin, F. Ishikawa, V. Hosur, B.L. Lyons, D.L. Greiner, Subcapsular transplantation of tissue in the kidney, Cold Spring Harb. Protoc. (2014) 737–740, https://doi.org/10.1101/pdb.prot078089.

[29] T.D. Schmittgen, K.J. Livak, Analyzing real-time PCR data by the comparative CT method, Nat. Protoc. 3 (2008) 1101–1108, https://doi.org/10.1038/nprot.2008.73.

[30] M.M. Moisenovich, A.Y. Arkhipova, A.A. Orlova, M.S. Drutskaya, S.V. Volkova, Composite scaffolds containing silk fibroin, gelatin, and hydroxyapatite for bone tissue regeneration and 3D cell culturing, Acta Naturae 6 (2014) 96–101.

[31] P. Couture, J. Paradis-Massie, N. Oualha, G. Thibault, Adhesion and transcellular migration of neutrophils and B lymphocytes on fibroblasts, Exp. Cell Res. 315 (2009) 2192–2206, https://doi.org/10.1016/j.yexcr.2009.04.013.

[32] C. Bénézech, A. White, E. Mader, K. Serre, S. Parnell, K. Pfeffer, C.F. Ware, G. Anderson, J.H. Caamaño, Ontogeny of stromal organizer cells during lymph node development, J. Immunol. 184 (2010) 4521–4530, https://doi.org/10.4049/jimmunol.0903113.Ontogeny.

[33] J. Greenwood, Y. Wang, V.L. Calder, Lymphocyte adhesion and transendothelial migration in the central nervous system: the role of LFA-1, ICAM-1, VLA-4 and VCAM-1. off, Immunology 86 (1995) 408–415.

[34] C. Berlin-Rufenach, F. Otto, M. Mathies, J. Westermann, M.J. Owen, A. Hamann, N. Hogg, Lymphocyte migration in lymphocyte function-associated antigen (LFA)-1-deficient mice, J. Exp. Med. 189 (1999) 1467–1478, https://doi.org/10.1084/jem.189.9.1467.

[35] A. Teijeira, M.C. Hunter, E. Russo, S.T. Proulx, T. Frei, G.F. Debes, M. Coles, I. Melero, M. Detmar, A. Rouzaut, C. Halin, T cell migration from inflamed skin to draining lymph nodes requires intralymphatic crawling supported by ICAM-1/LFA-1 interactions, Cell Rep. 18 (2017) 857–865, https://doi.org/10.1016/j.celrep.2016.12.078.

[36] J. Fu, D.A. Wang, In situ organ-specific vascularization in tissue engineering, Trends Biotechnol. 36 (2018) 834–849, https://doi.org/10.1016/j.tibtech.2018.02.012.
[37] M.P. Ruiz-Torres, G. Pérez-Rivero, M. Rodríguez-Puyol, D. Rodríguez-Puyol, M. L. Díez-Marqués, The leukocyte-endothelial cell interactions are modulated by extracellular matrix proteins, Cell. Physiol. Biochem. 17 (2006) 221–232, https://doi.org/10.1159/000094127.
[38] K.A. Roebuck, A. Rahman, V. Lakshminarayanan, K. Janakidevi, A.B. Malik, H2O2 and tumor necrosis factor-α activate intercellular adhesion molecule 1 (ICAM-1) gene transcription through distinct cis-regulatory elements within the ICAM-1 promoter, J. Biol. Chem. 270 (1995) 18966–18974, https://doi.org/10.1074/jbc.270.32.18966.
[39] T. Collins, M.A. Read, A.S. Neish, M.Z. Whitley, D. Thanos, T. Maniatis, Transcriptional regulation of endothelial cell adhesion molecules: NF-kappa B and cytokine-inducible enhancers, FASEB J. Off. Publ. Fed. Am. Soc. Exp. Biol. 9 (1995) 899–909.
[40] T.N. Ramos, D.C. Bullard, S.R. Barnum, ICAM-1: isoforms and phenotypes, J. Immunol. 192 (2014) 4469–4474, https://doi.org/10.4049/jimmunol.1400135.
[41] Y.-M. Lin, Z.-L. Chang, Y.-Y. Liao, M.-C. Chou, C.-H. Tang, IL-6 promotes ICAM-1 expression and cell motility in human osteosarcoma, Canc. Lett. 328 (2013) 135–143, https://doi.org/10.1016/j.canlet.2012.08.029.
[42] B.S. Wung, C.W. Ni, D.L. Wang, ICAM-1 induction by TNFalpha and IL-6 is mediated by distinct pathways via Rac in endothelial cells, J. Biomed. Sci. 12 (2005) 91–101, https://doi.org/10.1007/s11373-004-8170-z.
[43] C.W. Marlor, D.L. Webb, M.P. Bombara, J.M. Greve, M.L. Blue, Expression of vascular cell adhesion molecule-1 in fibroblastlike synoviocytes after stimulation with tumor necrosis factor, Am. J. Pathol. 140 (1992) 1055–1060.
[44] A.Y. Arkhipova, M.A. Nosenko, N.V. Malyuchenko, R.V. Zvartsev, A. M. Moisenovich, A.S. Zhdanova, T.V. Vasil'eva, E.A. Gorshkova, I.I. Agapov, M. S. Drutskaya, S.A. Nedospasov, M.M. Moisenovich, Effects of fibroin microcarriers on inflammation and regeneration of deep skin wounds in mice, Biochemistry 81 (2016) 1251–1260, https://doi.org/10.1134/S0006297916110031.
[45] M.M. Moisenovich, E.Y. Plotnikov, A.M. Moysenovich, D.N. Silachev, T.I. Danilina, E.S. Savchenko, M.M. Bobrova, L.A. Safonova, V. V Tatarskiy, M.S. Kotliarova, I. I. Agapov, D.B. Zorov, Effect of silk fibroin on neuroregeneration after traumatic brain injury, Neurochem. Res. 44 (10) (2019) 2261–2272, https://doi.org/10.1007/s11064-018-2691-8.
[46] J. Glowacki, S. Mizuno, Collagen scaffolds for tissue engineering, Biopolymers 89 (2008) 338–344, https://doi.org/10.1002/bip.20871.
[47] F.J. O'Brien, Biomaterials & scaffolds for tissue engineering, Mater. Today 14 (2011) 88–95, https://doi.org/10.1016/S1369-7021(11)70058-X.
[48] B.N. Brown, S.F. Badylak, Biocompatibility and immune response to biomaterials, in: Regen. Med. Appl. Organ Transplant., Elsevier, 2014, pp. 151–162, https://doi.org/10.1016/B978-0-12-398523-1.00011-2.
[49] M.A. Hendley, K.P. Murphy, C. Isely, H.L. Struckman, P. Annamalai, R.M. Gower, The Host Response to Poly(lactide-Co-Glycolide) Scaffolds Protects Mice from Diet Induced Obesity and Glucose Intolerance, Biomaterials, 2019, p. 119281, https://doi.org/10.1016/j.biomaterials.2019.119281.
[50] J. Yuan, B.O.A. Botchway, Y. Zhang, X. Wang, X. Liu, Combined bioscaffold with stem cells and exosomes can improve traumatic brain injury, Stem Cell Rev. Reports. 16 (2020) 323–334, https://doi.org/10.1007/s12015-019-09927-x.
[51] G.H. Altman, F. Diaz, C. Jakuba, T. Calabro, R.L. Horan, J. Chen, H. Lu, J. Richmond, D.L. Kaplan, Silk-based biomaterials, Biomaterials 24 (2003) 401–416. http://www.ncbi.nlm.nih.gov/pubmed/23896003.
[52] J. Melke, S. Midha, S. Ghosh, K. Ito, S. Hofmann, Silk fibroin as biomaterial for bone tissue engineering, Acta Biomater. 31 (2016) 1–16, https://doi.org/10.1016/j.actbio.2015.09.005.
[53] D. Jao, X. Mou, X. Hu, Tissue regeneration: a silk road, J. Funct. Biomater. 7 (2016) 22, https://doi.org/10.3390/jfb7030022.
[54] N. Johari, L. Moroni, A. Samadikuchaksaraei, Tuning the conformation and mechanical properties of silk fibroin hydrogels, Eur. Polym. J. 134 (2020) 109842, https://doi.org/10.1016/j.eurpolymj.2020.109842.
[55] A. Lazaris, S. Arcidiacono, Y. Huang, J.-F. Zhou, F. Duguay, N. Chretien, E. A. Welsh, J.W. Soares, C.N. Karatzas, Spider silk fibers spun from soluble recombinant silk produced in mammalian cells, Science 84 295 (2002) 472–476, https://doi.org/10.1126/science.1065780.
[56] S. Sangkert, J. Meesane, S. Kamonmattayakul, W.L. Chai, Modified silk fibroin scaffolds with collagen/decellularized pulp for bone tissue engineering in cleft palate: morphological structures and biofunctionalities, Mater. Sci. Eng. C 58 (2016) 1138–1149, https://doi.org/10.1016/j.msec.2015.09.031.
[57] Y.Y. Wu, Y.P. Jiao, L.L. Xiao, M.M. Li, H.W. Liu, S.H. Li, X. Liao, Y.T. Chen, J.X. Li, Y. Zhang, Experimental study on effects of adipose-derived stem cell-seeded silk fibroin chitosan film on wound healing of a diabetic rat model, Ann. Plast. Surg. 80 (2018) 572–580, https://doi.org/10.1097/SAP.0000000000001355.
[58] L. Yang, M. Yaseen, X. Zhao, P. Coffey, F. Pan, Y. Wang, H. Xu, J. Webster, J.R. Lu, Gelatin modified ultrathin silk fibroin films for enhanced proliferation of cells, Biomed. Mater. 10 (2015) 25003, https://doi.org/10.1088/1748-6041/10/2/025003.
[59] M.J. Rodriguez, J. Brown, J. Giordano, S.J. Lin, F.G. Omenetto, D.L. Kaplan, Silk based bioinks for soft tissue reconstruction using 3-dimensional (3D) printing with in vitro and in vivo assessments, Biomaterials 117 (2017) 105–115, https://doi.org/10.1016/j.biomaterials.2016.11.046.
[60] Y.R. Park, M.T. Sultan, H.J. Park, J.M. Lee, H.W. Ju, O.J. Lee, D.J. Lee, D.L. Kaplan, C.H. Park, NF-κB signaling is key in the wound healing processes of silk fibroin, Acta Biomater. 67 (2017) 183–195, https://doi.org/10.1016/j.actbio.2017.12.006.
[61] W. Chen, B. Tian, J. Liang, S. Yu, Y. Zhou, S. Li, Matrix stiffness regulates the interactions between endothelial cells and monocytes, Biomaterials 221 (2019) 119362, https://doi.org/10.1016/j.biomaterials.2019.119362.
[62] D. Bagrov, V. Zhuikov, Y. Chudinova, A. Yarisheva, M. Kotlyarova, A. Arkhipova, D. Khaydapova, M. Moisenovich, K. Shaitan, Mechanical properties of films and three-dimensional scaffolds made of fibroin and gelatin, Biophysics 62 (2017) 17–23, https://doi.org/10.1134/S0006350917010031.
[63] E. Pérez Del Río, M. Martinez Miguel, J. Veciana, I. Ratera, J. Guasch, Artificial 3D culture systems for T cell expansion, ACS Omega 3 (2018) 5273–5280, https://doi.org/10.1021/acsomega.8b00521.
[64] P. Bertolino, A. Schrage, D.G. Bowen, K. Klugewitz, S. Ghani, K. Eulenburg, L. Holz, N. Hogg, G.W. McCaughan, A. Hamann, Early intrahepatic antigen-specific retention of naïve CD8+ T cells is predominantly ICAM-1/LFA-1 dependent in mice, Hepatology 42 (2005) 1063–1071, https://doi.org/10.1002/hep.20885.
[65] J.W. Griffith, C.L. Sokol, A.D. Luster, Chemokines and chemokine receptors: positioning cells for host defense and immunity, Annu. Rev. Immunol. 32 (2014) 659–702, https://doi.org/10.1146/annurev-immunol-032713-120145.
[66] S.N. Mueller, K.A. Hosiawa-Meagher, B.T. Konieczny, B.M. Sullivan, M. F. Bachmann, R.M. Locksley, R. Ahmed, M. Matloubian, Regulation of homeostatic chemokine expression and cell trafficking during immune responses, Science 80– (2007) 670–675. http://www.sciencemag.org/content/317/5838/670.short. (Accessed 14 January 2015).
[67] S. Suematsu, T. Watanabe, Generation of a synthetic lymphoid tissue-like organoid in mice, Nat. Biotechnol. 22 (2004) 1539–1545, https://doi.org/10.1038/nbt1039.
[68] Y. Kobayashi, T. Watanabe, Synthesis of artificial lymphoid tissue with immunological function, Trends Immunol. 31 (2010) 422–428, https://doi.org/10.1016/j.it.2010.09.002.
[69] Y. Kobayashi, T. Watanabe, Gel-trapped lymphorganogenic chemokines trigger artificial tertiary lymphoid organs and mount adaptive immune responses in vivo, Front. Immunol. 7 (2016) 316, https://doi.org/10.3389/fimmu.2016.00316.
[70] A.J. Najibi, D.J. Mooney, Cell and tissue engineering in lymph nodes for cancer immunotherapy, Adv. Drug Deliv. Rev. 161–162 (2020) 42–62, https://doi.org/10.1016/j.addr.2020.07.023.